Appl. Math. Mech. -Engl. Ed., **43**(10), 1543–1554 (2022)

APPLIED MATHEMATICS AND MECHANICS (ENGLISH EDITION)

https://doi.org/10.1007/s10483-022-2904-9

Multiple internal resonances of rotating composite cylindrical shells under varying temperature fields*

Yunfei LIU, Jun WANG, Jiaxin HU, Zhaoye QIN†, Fulei CHU

State Key Laboratory of Tribology, Department of Mechanical Engineering, Tsinghua University, Beijing 100084, China

(Received Apr. 9, 2022 / Revised Jul. 13, 2022)

Abstract Composite cylindrical shells, as key components, are widely employed in large rotating machines. However, due to the frequency bifurcations and dense frequency spectra caused by rotation, the nonlinear vibration usually has the behavior of complex multiple internal resonances. In addition, the varying temperature fields make the responses of the system further difficult to obtain. Therefore, the multiple internal resonances of composite cylindrical shells with porosities induced by rotation with varying temperature fields are studied in this paper. Three different types of the temperature fields, the Coriolis forces, and the centrifugal force are considered here. The Hamilton principle and the modified Donnell nonlinear shell theory are used to obtain the equilibrium equations of the system, which are transformed into the ordinary differential equations (ODEs) by the multi-mode Galerkin technique. Thereafter, the pseudo-arclength continuation method, which can identify the regions of instability, is introduced to obtain the numerical results. The detailed parametric analysis of the rotating composite shells is performed. Multiple internal resonances caused by the interaction between backward and forward wave modes and the energy transfer phenomenon are detected. Besides, the nonlinear amplitude-frequency response curves are different under different temperature fields.

Key words multiple internal resonances, rotation effect, nonlinear temperature variation, multi-mode Galerkin technique, pseudo-arclength continuation method, coupled effect

Chinese Library Classification O322
2010 Mathematics Subject Classification 74H45

1 Introduction

Composite materials have the advantages of high specific stiffness, specific strength, and good vibration reduction performance, which are widely used in various engineering fields[1–5]. Rotating thin structures, as a key basic structure, have been employed in mechanical, civil, and aerospace engineering[6–9]. Due to the anisotropy, Coriolis, and centrifugal effects, the vibration behaviors of rotating composite structures must be different from those of homogeneous

* Citation: LIU, Y. F., WANG, J., HU, J. X., QIN, Z. Y., and CHU, F. L. Multiple internal resonances of rotating composite cylindrical shells under varying temperature fields. *Applied Mathematics and Mechanics* (*English Edition*), **43**(10), 1543–1554 (2022) https://doi.org/10.1007/s10483-022-2904-9

† Corresponding author, E-mail: qinzy@mail.tsinghua.edu.cn

Project supported by the National Natural Science Foundation of China (No. 11972204)

stationary structures. Hence, it is of great significance to carry out analysis and research on the dynamic responses of rotating composite thin structures for guiding the corresponding engineering applications. To date, the vibration analysis of rotating composite structures has been investigated by many scholars[10–12].

When mechanical systems such as rotor systems generate vibrations, the resonances of the structures such as rotating shells can be caused by appropriate geometrical parameters or rotation effect, and thus the large amplitude vibrations of these structures may occur under the transverse loads[13–15]. It affects the normal operation of the rotating structures seriously. Therefore, the study on nonlinear large amplitude vibrations is very important for the reliability and safety of the equipment, and the nonlinear vibration cannot be ignored in this case[16–20].

There are some investigations on the nonlinear dynamic responses of rotating composite structures. A simplified mathematical model to study the nonlinear vibrations of rotating composite beams was established by Rafiee et al.[21]. Gu et al.[22] performed the nonlinear vibration of graphene platelets reinforced pre-twisted composite blades. Li et al.[23] reported the nonlinear vibrations of rotating composite shells under arbitrary boundary conditions.

Moreover, it is worth noting that all the above studies did not consider the influence of the temperature. Actually, the working environment of these rotating structures is usually with varying temperature fields, and the temperature will greatly affect the mechanical properties. Considering the thermal effect, Khosravi et al.[24] analyzed the vibration behavior of carbon nanotube reinforced rotating composite beams, and found that the instability of the rotating composite beam under the hinged-clamped boundary conditions could be caused by a decrease in the temperature. Considering the hygro-thermal effect, Li et al.[25] proposed a general approach for dealing with the thermal vibration characteristics of functionally graded porous stepped cylindrical shells. Liu et al.[26] demonstrated that the nonlinear vibrations of rotating composite eccentric shells were significantly influenced by the external loads, the rotating speed, and the temperature.

Based on the literature review, there are just a few studies on the dynamic response of rotating composite structures under the thermal load. There is no literature available to deal with the multiple internal resonances of composite shells with porosities induced by rotation under various temperature fields. Hence, this paper aims to reveal the complex mechanisms of multiple internal resonances and the energy transfer phenomena caused by rotation, and to conduct the effect of varying temperature fields on the nonlinear vibration characteristics. The Hamilton principle and modified Donnell nonlinear shell theory are used to gain the equilibrium equations, which are then transformed into nonlinear ordinary differential equations (ODEs) by utilizing the multi-mode Galerkin technique. The pseudo-arclength continuation method is introduced to obtain accurate results. The effects of key parameters on multiple internal resonances of rotating composite shells are studied.

2 Rotating composite shell model under various thermal loads

In this study, a rotating composite thin shell with a constant rotating speed Ω is made of ceramic and metal, and the geometry of the shell is presented in Fig. 1. The material properties vary by gradient from inside to outside, in which the inner and outer surfaces are metal and ceramic, respectively. Porosities are considered here due to the manufacturing process. The rotating composite thin shell is under external harmonic excitation and various temperature fields, wherein three different types of temperature field distributions, namely, uniform temperature (UT) variation, linear temperature (LT) variation, and nonlinear linear temperature (NLT) variation, are studied here as representative temperature fields.

Case 1 UT variation

At the initial reference Kelvin temperature T_0, the temperature of the entire composite thin

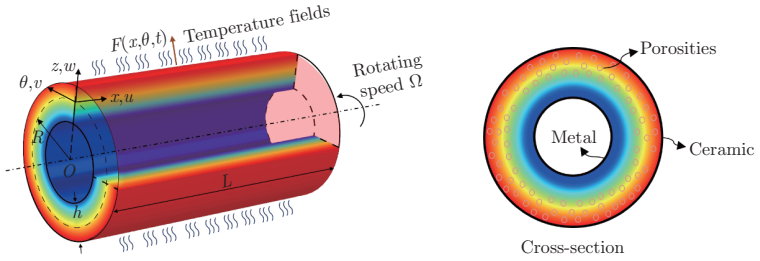

Fig. 1 Schematic views of a rotating functionally graded composite shell with porosities under various temperature fields (color online)

shell is approximated to rise uniformly to a final value T, and the process can be given by

$$T = T_0 + \Delta T, \tag{1}$$

in which ΔT denotes the temperature difference between the initial state and the final state.

Case 2 LT variation

Assume that the temperature difference changes linearly along the thickness. Then, the temperature expression can be given by

$$T(z) = T_0 + \Delta T\Big(\frac{z}{h} + \frac{1}{2}\Big). \tag{2}$$

Case 3 NLT variation

The temperature is considered to be a nonlinear change along the shell thickness direction. Due to the lack of a heat source, a one-dimensional steady-state heat transfer equation is satisfied as follows:

$$\frac{\mathrm{d}}{\mathrm{d}z}\Big(\kappa(z)\frac{\mathrm{d}T}{\mathrm{d}z}\Big) = 0, \tag{3}$$

and the boundary condition is

$$T(z) = \begin{cases} T_{\mathrm{c}}, & z = \dfrac{h}{2}, \\ T_{\mathrm{m}}, & z = -\dfrac{h}{2}, \end{cases} \tag{4}$$

where c and m denote ceramic and metal, respectively, $\kappa(z)$ denotes the thermal conductivity, and the non-uniformity of thermal conductivity is given in a power form as

$$\kappa(z) = (\kappa_{\mathrm{c}} - \kappa_{\mathrm{m}})\Big(\frac{z}{h} + \frac{1}{2}\Big)^N + \kappa_{\mathrm{m}}, \tag{5}$$

where $N \in [0, \infty)$ denotes the power-law index.

By solving Eqs. (3)–(5), the solution of temperature variation T as a nonlinear function of the thickness z can be obtained.

The temperature-dependent material parameters are

$$P = P_0(P_3T^3 + P_2T^2 + P_1T + P_{-1}T^{-1} + 1), \tag{6}$$

in which P_3, P_2, P_1, P_{-1}, and P_0 stand for the temperature coefficients of the constituent materials.

Due to manufacturing defects, porosities are usually not evenly distributed in the material, and they are abundant in the middle plane and dissipate gradually towards both ends[27]. Therefore, the effective material parameter is modified as

$$P(z,T) = P_{\mathrm{c}}(T)\Big(V_{\mathrm{c}}(z) - \frac{\alpha}{2}\Big(1 - \frac{2|z|}{h}\Big)\Big) + P_{\mathrm{m}}(T)\Big(V_{\mathrm{m}}(z) - \frac{\alpha}{2}\Big(1 - \frac{2|z|}{h}\Big)\Big), \tag{7}$$

where V_{m} and P_{m} denote the volume fraction and material property of metal, respectively, V_{c} and P_{c} denote those of ceramic, respectively, and $\alpha\,(\alpha \ll 1)$ denotes the porosity volume fraction.

The sum of the two volume fractions is $V_{\mathrm{m}}(z) + V_{\mathrm{c}}(z) = 1$. The volume fraction of the rotating composite shell, which obeys the power-law distribution, changes along the thickness direction as

$$V_{\mathrm{c}}(z) = \Big(\frac{2z+h}{2h}\Big)^N. \tag{8}$$

As for the rotating composite thin shell with uneven porosity distribution, the effective material parameter can be rewritten as

$$P(z,T) = P_{\mathrm{m}}(T) + (P_{\mathrm{c}}(T) - P_{\mathrm{m}}(T))\Big(\frac{2z+h}{2h}\Big)^N - \frac{\alpha}{2}(P_{\mathrm{m}}(T) + P_{\mathrm{c}}(T))\Big(\frac{h-2|z|}{h}\Big), \tag{9}$$

where the material property P denotes the general mass density ρ, the elastic modulus E, Poisson's ratio ν, or the thermal expansion coefficient α_{T}.

An improved Donnell nonlinear shell theory, which has better accuracy under small circumferential wave numbers, is adopted, where the strain-displacement relation is

$$\begin{bmatrix}\varepsilon_{xx}\\ \varepsilon_{\theta\theta}\\ \gamma_{x\theta}\end{bmatrix} = \begin{bmatrix}\dfrac{\partial u}{\partial x} + \dfrac{1}{2}\Big(\dfrac{\partial w}{\partial x}\Big)^2\\ \dfrac{1}{R}\Big(\dfrac{\partial v}{\partial \theta} + w\Big) + \dfrac{1}{2}\Big(\dfrac{\partial w}{R\partial \theta}\Big)^2\\ \dfrac{\partial v}{\partial x} + \dfrac{1}{R}\dfrac{\partial u}{\partial \theta} + \dfrac{1}{R}\dfrac{\partial w}{\partial \theta}\dfrac{\partial w}{\partial x}\end{bmatrix} - z\begin{bmatrix}\dfrac{\partial^2 w}{\partial x^2}\\ \Big(\dfrac{\partial^2 w}{R^2\partial \theta^2} - \dfrac{\partial v}{R^2\partial \theta}\Big)\\ 2\Big(\dfrac{\partial^2 w}{R\partial x\partial \theta} - \dfrac{\partial v}{R\partial x}\Big)\end{bmatrix}. \tag{10}$$

The stress-strain relation considering the thermal effect is[28]

$$\begin{bmatrix}\sigma_{xx}\\ \sigma_{\theta\theta}\\ \sigma_{x\theta}\end{bmatrix} = \begin{bmatrix}C_{11} & C_{12} & 0\\ C_{21} & C_{22} & 0\\ 0 & 0 & C_{66}\end{bmatrix}\left(\begin{bmatrix}\varepsilon_{xx}\\ \varepsilon_{\theta\theta}\\ \gamma_{x\theta}\end{bmatrix} - \begin{bmatrix}\alpha_{\mathrm{T}}(z,T)\\ \alpha_{\mathrm{T}}(z,T)\\ 0\end{bmatrix}\Delta T\right), \tag{11}$$

where

$$C_{11} = C_{22} = \frac{E(z,T)}{1-\nu(z,T)^2}, \quad C_{12} = C_{21} = \frac{E(z,T)\nu(z,T)}{1-\nu(z,T)^2}, \quad C_{66} = \frac{E(z,T)}{2(1+\nu(z,T))}. \tag{12}$$

By using the Hamilton principle, the partial differential equations considering the structure damping coefficient c_{d} are obtained as

$$\frac{\partial N_x}{\partial x} + \frac{\partial N_{x\theta}}{R\partial \theta} + I_0\Omega^2\frac{\partial^2 u}{\partial \theta^2} = I_0\frac{\partial^2 u}{\partial t^2}, \tag{13}$$

$$\begin{aligned}&\frac{\partial N_{x\theta}}{\partial x} + \frac{1}{R}\frac{\partial N_\theta}{\partial \theta} + \frac{2}{R}\frac{\partial M_{x\theta}}{\partial x} + \frac{1}{R^2}\frac{\partial M_\theta}{\partial \theta} - I_0\Omega^2 v + 2I_0\Omega^2\frac{\partial w}{\partial \theta} + I_0\Omega^2\frac{\partial^2 v}{\partial \theta^2}\\ =\,&2I_0\Omega\frac{\partial w}{\partial t} - I_0\Omega^2 v + I_0\frac{\partial^2 v}{\partial t^2},\end{aligned} \tag{14}$$

$$\begin{aligned}&-\frac{N_\theta}{R} + \frac{1}{R^2}\frac{\partial N_\theta}{\partial \theta}\frac{\partial w}{\partial \theta} + \frac{1}{R^2}\frac{\partial^2 M_\theta}{\partial \theta^2} + \frac{N_\theta}{R^2}\frac{\partial^2 w}{\partial \theta^2} + \frac{\partial N_{x\theta}}{\partial x}\frac{\partial w}{R\partial \theta}\\ &+ \frac{\partial N_{x\theta}}{R\partial \theta}\frac{\partial w}{\partial x} + \frac{\partial N_x}{\partial x}\frac{\partial w}{\partial x} + 2\frac{\partial^2 M_{x\theta}}{R\partial x\partial \theta} + 2N_{x\theta}\frac{\partial^2 w}{R\partial x\partial \theta} + \frac{\partial^2 M_x}{\partial x^2}\\ &+ N_x\frac{\partial^2 w}{\partial x^2} - c_{\mathrm{d}}h\frac{\partial w}{\partial t} - I_0\Omega^2 w - 2I_0\Omega^2\frac{\partial v}{\partial \theta} + I_0\Omega^2\frac{\partial^2 w}{\partial \theta^2}\\ =\,&I_0\frac{\partial^2 w}{\partial t^2} - F(t) - I_0\Omega^2 w - 2I_0\Omega\frac{\partial v}{\partial t},\end{aligned} \tag{15}$$

where

$$\begin{cases} [N_x, N_\theta, N_{x\theta}] = \displaystyle\int_{-h/2}^{h/2} [\sigma_{xx}, \sigma_{\theta\theta}, \sigma_{x\theta}] \mathrm{d}z, \quad [M_x, M_\theta, M_{x\theta}] = \int_{-h/2}^{h/2} [\sigma_{xx}, \sigma_{\theta\theta}, \sigma_{x\theta}] z \mathrm{d}z, \\ I_0 = \displaystyle\int_{-h/2}^{h/2} \rho(z, T) \mathrm{d}z, \quad F(t) = f\delta(x - x_0)\delta(R(\theta - \theta_0)) \cos(\omega_f t), \end{cases} \tag{16}$$

in which f represents the amplitude of the radial force, (x_0, θ_0) denotes the point at which the radial force is applied, δ represents the Dirac delta function, and ω_f denotes the excitation frequency.

3 Solution method

For a cylindrical shell simply supported at both ends, to discretize this system, the displacement functions are[29]

$$\begin{aligned} u(x, \theta, t) = & \sum_{m=1}^{M_1} \sum_{n=1}^{N_1} (u_{m,n,c}(t) \cos(n\theta) + u_{m,n,s}(t) \sin(n\theta)) \cos \frac{m\pi x}{L} \\ & + \sum_{m=1}^{M_2} u_{2m-1,0}(t) \cos \frac{(2m-1)\pi x}{L}, \end{aligned} \tag{17}$$

$$v(x, \theta, t) = \sum_{m=1}^{M_1} \sum_{n=1}^{2N_1} (v_{m,n,c}(t) \sin(n\theta) + v_{m,n,s}(t) \cos(n\theta)) \sin \frac{m\pi x}{L}, \tag{18}$$

$$\begin{aligned} w(x, \theta, t) = & \sum_{m=1}^{M_1} \sum_{n=1}^{N_1} (w_{m,n,c}(t) \cos(n\theta) + w_{m,n,s}(t) \sin(n\theta)) \sin \frac{m\pi x}{L} \\ & + \sum_{m=1}^{M_2} w_{2m-1,0}(t) \sin \frac{(2m-1)\pi x}{L}, \end{aligned} \tag{19}$$

where $u_{m,n}(t)$, $v_{m,n}(t)$, and $w_{m,n}(t)$ denote the displacement amplitude components, and M_1 and N_1 represent the truncated coefficients. The subscript c represents the driving mode, and the subscript s represents the companion mode.

Substitute Eqs. (17)–(19) into Eqs. (13)–(15) and then transform the motion equations into nonlinear ODEs by using the multi-mode Galerkin technique. The detailed derivation process can be found in Refs. [30] and [31].

The system of nonlinear coupled ODEs is expressed in a matrix form as

$$\boldsymbol{M}\ddot{X} + \boldsymbol{C}\dot{X} + \boldsymbol{K}X + \boldsymbol{G}\dot{X} + \boldsymbol{\Gamma}(X) = \boldsymbol{F}(t), \tag{20}$$

where $X = [u, v, w]^{\mathrm{T}}$, $\boldsymbol{M}$, $\boldsymbol{C}$, and $\boldsymbol{K}$ indicate the mass, the damping, and the stiffness matrices, respectively, $\boldsymbol{\Gamma}$ denotes the other nonlinear parts such as the temperature non-linearity, $\boldsymbol{G}$ represents the gyroscopic matrix caused by the rotation, and $\boldsymbol{F}$ denotes the vector of external force. Since these matrices all have very tedious expressions, they are not stated here.

Since the moments of inertia of the displacements u and v have little impact on the radial response, they are not considered here. Therefore, the results can be substituted into Eq. (15) to obtain the nonlinear ODEs only related to w.

Then, the pseudo-arclength continuation technique can be applied to solve the nonlinear ODEs on the software MATCONT[32]. This method can be extended to analyze shell structures with different geometric shapes and boundary conditions by establishing the corresponding shell displacement functions.

4 Results and discussion

First, the dimensionless frequency of a rotating infinitely long thin shell is compared with that obtained by Chen et al.[33] as shown in Table 1. The dimensionless forward and backward traveling wave frequencies in the table are, respectively, expressed by ω^*_{ft} and ω^*_{bt}. The comparison shows that the derivation in this paper is correct, and the proposed method can effectively analyze the traveling wave vibrations of rotating shells.

Table 1 Comparison of dimensionless frequencies of a rotating infinitely long thin shell at the room temperature, when $h/R = 0.02$, $\nu = 0.3$, $\omega^{*2} = \rho R^2(1-\nu^2)\omega^2/E$, and $\Omega^{*2} = \rho R^2(1-\nu^2)\Omega^2/E$

Ω^*	n	Chen et al.[33]		Present	
		ω^*_{bt}	ω^*_{ft}	ω^*_{bt}	ω^*_{ft}
0.000 5	2	0.015 90	0.015 10	0.015 90	0.015 10
	3	0.044 12	0.043 52	0.044 13	0.043 53
	4	0.084 25	0.083 78	0.084 27	0.083 79
	5	0.136 07	0.135 68	0.136 08	0.135 69
0.001 0	2	0.016 32	0.014 72	0.016 34	0.014 74
	3	0.044 43	0.043 23	0.044 48	0.043 28
	4	0.084 49	0.083 55	0.084 56	0.083 61
	5	0.136 26	0.135 49	0.136 33	0.135 56

The nonlinear vibration response curves of a stationary thin shell are further compared as presented in Fig. 2. The corresponding parameters adopted are $\rho = 2\,796$ kg/m^3, $E = 71.02 \times 10^9$ Pa, $\nu = 0.31$, $h = 0.247 \times 10^3$ m, $R = 0.1$ m, $L = 0.2$ m, $m = 1$, $n = 6$, and $f = 0.001\,2 I_0 h \omega^2_{0,mn}$, and the damping ratio $2\xi_{1,n} = 0.001$. It can be found that the results are consistent with those of Ref. [34].

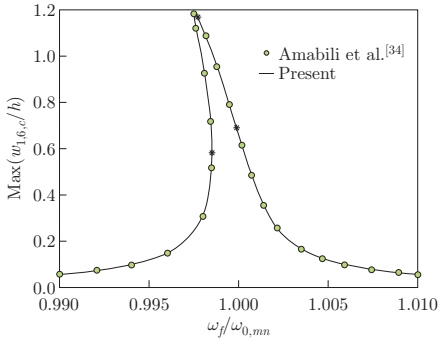

Fig. 2 Comparison of nonlinear amplitude-frequency response curves of a stationary thin shell at the room temperature (color online)

The material properties of the composite shell subject to various temperature fields are presented in Table 2. If not specified, the other parameters adopted are $L = 0.5$, $R = 1$, $h = 0.02$, $\Omega^* = 0.02$, $\alpha = 0.1$, $N = 1$, $T_{\mathrm{m}} = T_0 = 300\,\mathrm{K}$, $\Delta T = 300\,\mathrm{K}$, $(x_0, \theta_0) = (L/2, 0)$, $2\xi_{1,n} = 0.003$, and $f = f_0 I_0 h \omega^2_{0,(m=1,n=4)}$, where f_0 represents the modal excitation amplitude, and its value is 0.002. $\omega_{0,(m=1,n=4)}$ is the natural frequency of the mode ($m = 1$, $n = 4$) of a cylindrical shell without rotation. For the sake of simplicity, the subscript "($m = 1$, $n = 4$)" is ignored. In Fig. 3, with the rotating speed increasing, the forward wave frequency decreases slightly and increases subsequently, while the backward wave frequency keeps increasing. The fundamental frequency occurs at ($m = 1$, $n = 4$). Additionally, many intersection points are observed on the Campbell diagram at a specific wave number. As illustrated in Fig. 4,

the forward wave frequency in the mode ($m = 1$, $n = 4$) is the same as the backward wave frequency in the mode ($m = 1$, $n = 5$) at a specific rotating speed. Therefore, due to the rotation effect, the energy transfer between these two fundamental modes is likely to happen, and further nonlinear multiple resonance phenomena occur. In order to capture the peculiar phenomenon correctly, 50 degrees of freedom (DOFs) are considered here as follows: $u_{1,4,c}$, $u_{1,5,c}$, $u_{2,4,c}$, $u_{2,5,c}$, $u_{3,4,c}$, $u_{3,5,c}$, $v_{1,4,c}$, $v_{1,8,c}$, $v_{1,5,c}$, $v_{1,10,c}$, $v_{2,4,c}$, $v_{2,8,c}$, $v_{2,5,c}$, $v_{2,10,c}$, $v_{3,4,c}$, $v_{3,8,c}$, $v_{3,5,c}$, $v_{3,10,c}$, $w_{1,4,c}$, $w_{1,5,c}$, $w_{2,4,c}$, $w_{2,5,c}$, $u_{1,4,s}$, $u_{1,5,s}$, $u_{2,4,s}$, $u_{2,5,s}$, $u_{3,4,s}$, $u_{3,5,s}$, $v_{1,4,s}$, $v_{1,8,s}$, $v_{1,5,s}$, $v_{1,10,s}$, $v_{2,4,s}$, $v_{2,8,s}$, $v_{2,5,s}$, $v_{2,10,s}$, $v_{3,4,s}$, $v_{3,8,s}$, $v_{3,5,s}$, $v_{3,10,s}$, $w_{1,4,s}$, $w_{1,5,s}$, $w_{2,4,s}$, $w_{2,5,s}$, $u_{1,0}$, $u_{3,0}$, $u_{5,0}$, $w_{1,0}$, $w_{3,0}$, and $w_{5,0}$.

Table 2 Material properties of the rotating composite shell subject to various temperature fields

Material	Property	P_0	P_{-1}	P_1	P_2	P_3
Al_2O_3	E/Pa	349.550×10^9	0	-3.853×10^{-4}	-4.027×10^{-7}	-1.673×10^{-10}
	μ	0.26	0	0	0	0
	$\rho/(\mathrm{kg \cdot m^{-3}})$	3 950	0	0	0	0
	$\alpha_T/\mathrm{K^{-1}}$	$6.826\,9 \times 10^{-6}$	0	1.838×10^{-4}	0	0
	$\kappa/(\mathrm{W \cdot m^{-1} \cdot K^{-1}})$	−14.087	−1 123.6	-6.227×10^{-3}	0	0
Nickel	E/GPa	205.098×10^9	0	-2.794×10^{-4}	-3.998×10^{-9}	0
	μ	0.31	0	0	0	0
	$\rho/(\mathrm{kg \cdot m^{-3}})$	8 900	0	0	0	0
	$\alpha_T/\mathrm{K^{-1}}$	$9.920\,9 \times 10^{-6}$	0	8.705×10^{-4}	0	0
	$\kappa/(\mathrm{W \cdot m^{-1} \cdot K^{-1}})$	187.660	0	-2.869×10^{-3}	4.005×10^{-6}	-1.983×10^{-9}

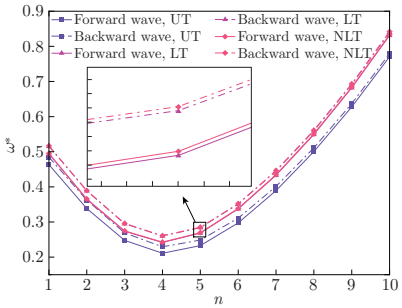

Fig. 3 Dimensionless frequency ω^* against circumferential wave number n of the rotating composite shell subject to various temperature fields ($\Omega^* = 0.02$) (color online)

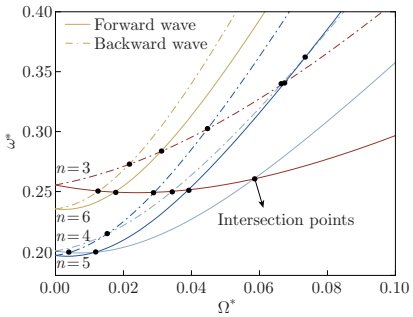

Fig. 4 Campbell diagram of the rotating composite shell in NLT variation (color online)

Figure 5 presents the nonlinear dynamic responses of the rotating composite thin shell subject to various temperature fields. There are four coupled peaks in the amplitude-frequency response curves due to the multiple internal resonances and rotating effect. The first peak is bending to the left, and the rest peaks turn to the right as the nonlinear frequency ratio increases, and the amplitude of the second peak is larger than that of the others. Besides, analysis shows that the bending of the dynamic response curves results in a jump phenomenon. The jump phenomenon implies a sudden change in amplitude, and the multiple amplitudes mean several resonance responses. In addition, the locations of the Neimark-Sacker (NS) bifurcation points and branch point of cycles (BPC) on the response curves vary with different temperature fields. However, the response curves under the NLT field and those under the LT field have little difference.

In Fig. 6, the nonlinear dynamic responses for different temperature variations are presented. The jump phenomenon occurs in these curves. It is known that the dynamic response curves of

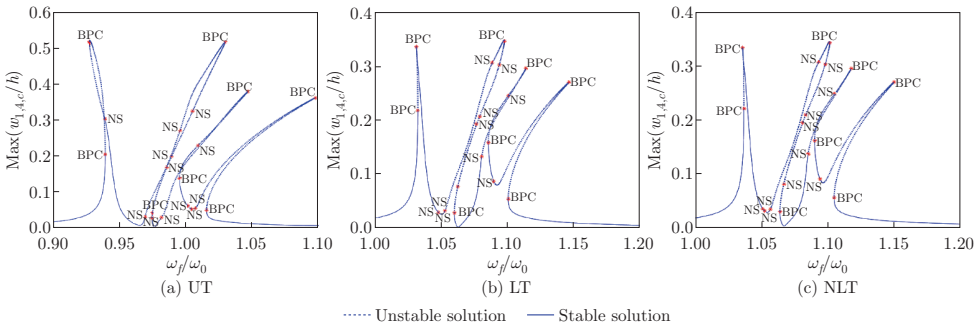

Fig. 5 Nonlinear amplitude-frequency response curves of the rotating composite shell subject to various temperature fields: (a) UT, (b) LT, and (c) NLT (color online)

the rotating composite shell bend to the left when they have softening property and to the right when they have hardening one. It is known that the nonlinear amplitude-frequency response curve of the rotating composite shell bends to the left and right when it has the softening and hardening characteristics, respectively. The resonance amplitudes increase significantly and the resonance region moves to the left with the increase in the temperature change. The results show that the energy increment induced by the temperature change has a notable effect on the dynamic responses. Besides, for the UT type, more peaks appear on the response curve by increasing the temperature change.

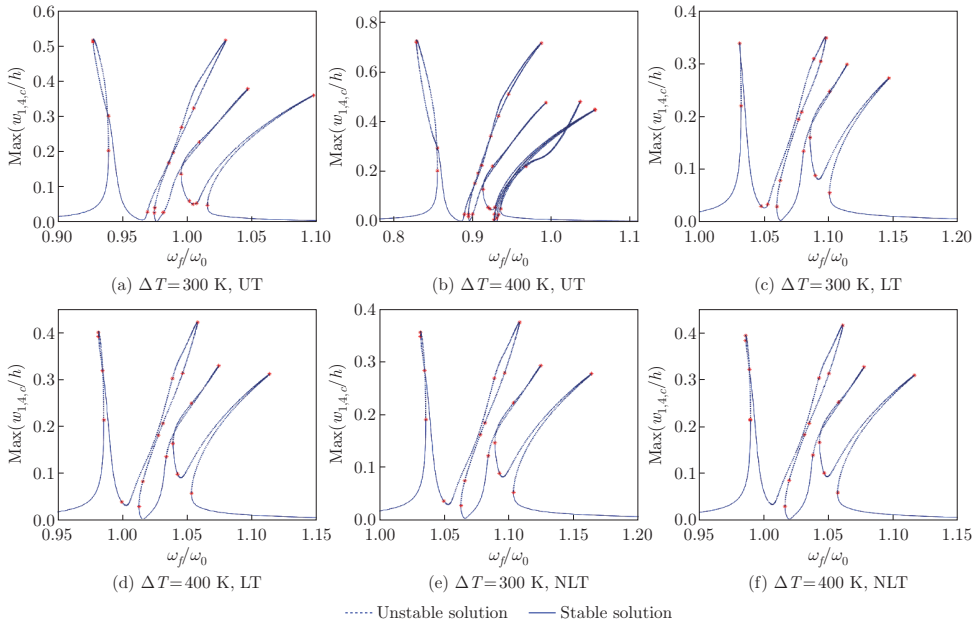

Fig. 6 Nonlinear amplitude-frequency response curves of the rotating composite shell for different temperature variations: (a), (c), and (e) $\Delta T = 300\,\mathrm{K}$; (b), (d), and (f) $\Delta T = 400\,\mathrm{K}$ (color online)

Figure 7 illustrates the nonlinear dynamic responses for different porosity volume fractions. Here, $\alpha = 0$ corresponds to the rotating composite shell without porosity. One can find that the porosity volume fraction has a notable effect on the nonlinear vibration behavior of the rotating composite thin shell. Examining Figs. 7(a) and 7(b) shows that the peaks with respect to the unstable solution decrease with the increase in the porosity. This is because that addition will lead to a decrease in the shell stiffness, consequently weakening the nonlinear coupling induced

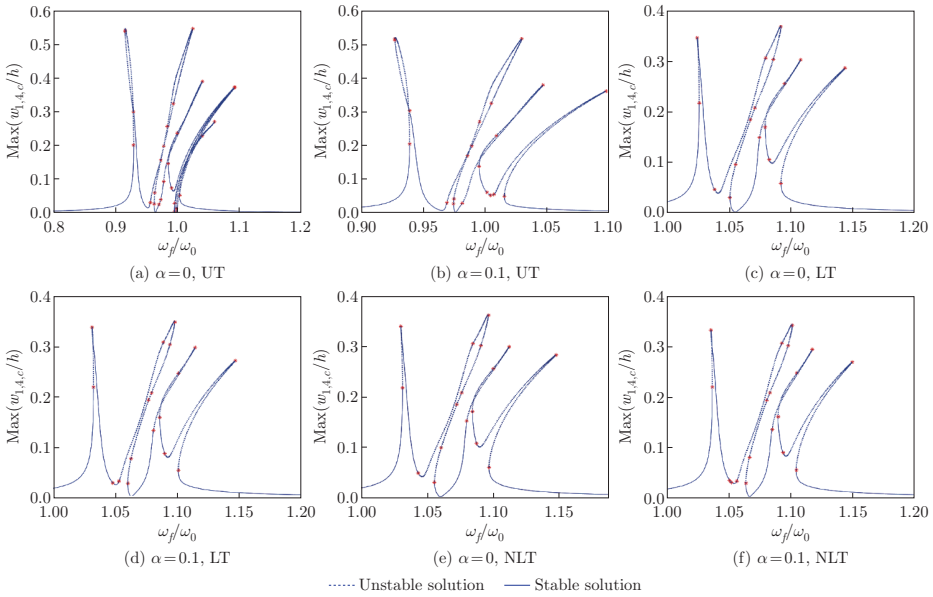

Fig. 7 Nonlinear amplitude-frequency response curves of the rotating composite shell for different porosity volume fractions: (a), (c), and (e) $\alpha = 0$; (b), (d), and (f) $\alpha = 0.1$ (color online)

by the large deformation of the rotating composite shell. Additionally, a trend is observed that the resonance region moves towards the direction of the larger dimensionless nonlinear frequency with the porosity volume fraction increasing.

The nonlinear dynamic responses for different power-law indexes are presented in Fig. 8. As the dimensionless nonlinear frequency increases, the amplitude peaks of the driving mode $w_{1,4,c}/h$ increase as the power-law index increases. At the same time, the partial stable solution on the first resonance peak is converted to an unstable solution for all the three temperature types. Furthermore, it is revealed from these figures that the resonance regions of the driven mode $w_{1,4,c}$ move to the lower dimensionless nonlinear frequency by increasing the power-law index.

As shown in Fig. 9, the nonlinear dynamic responses for different dimensionless rotating speeds are investigated. The results demonstrate that the nonlinear dynamic response curves are sensitive to the rotating speed. A very significant difference is that the nonlinear hardening/softening spring behaviors attenuate as the dimensionless rotating speed increases. That is because the increase in the rotating speed weakens the coupled effect between the modes. Moreover, as the rotating speed increases, the peak values of the nonlinear amplitude-frequency response curves gradually decrease, and the resonance regions move to the direction of the larger dimensionless nonlinear frequency.

5 Conclusions

The multiple internal resonances of composite cylindrical shells with porosities induced by rotation with varying temperature fields are investigated. It is shown that the nonlinear vibration response exhibits both hardening and softening characteristics, and four coupled peaks and an energy transfer phenomenon are detected due to the multiple internal resonances induced by the rotation effect. In addition, the locations of the BPC and NS points vary with the temperature fields, but the dynamic response curves under the NLT and LT fields have little difference. Besides, the energy increment induced by the temperature variation has notable influence on the nonlinear dynamic responses. For the UT type, more peaks appear on the response curves as the temperature change increases. Furthermore, the resonance region moves

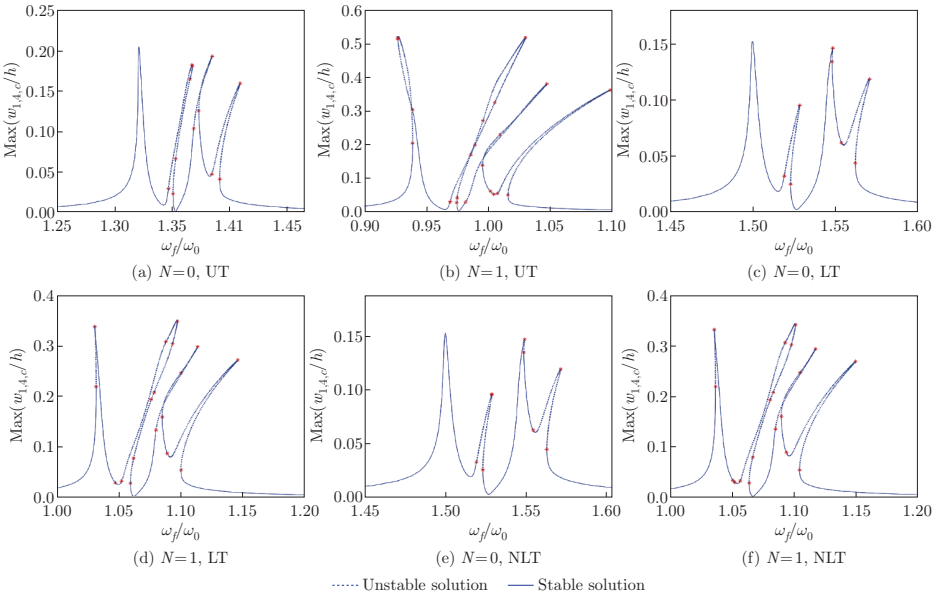

Fig. 8 Nonlinear amplitude-frequency response curves of the rotating composite shell for different power-law indexes: (a), (c), and (e) $N = 0$; (b), (d), and (f) $N = 1$ (color online)

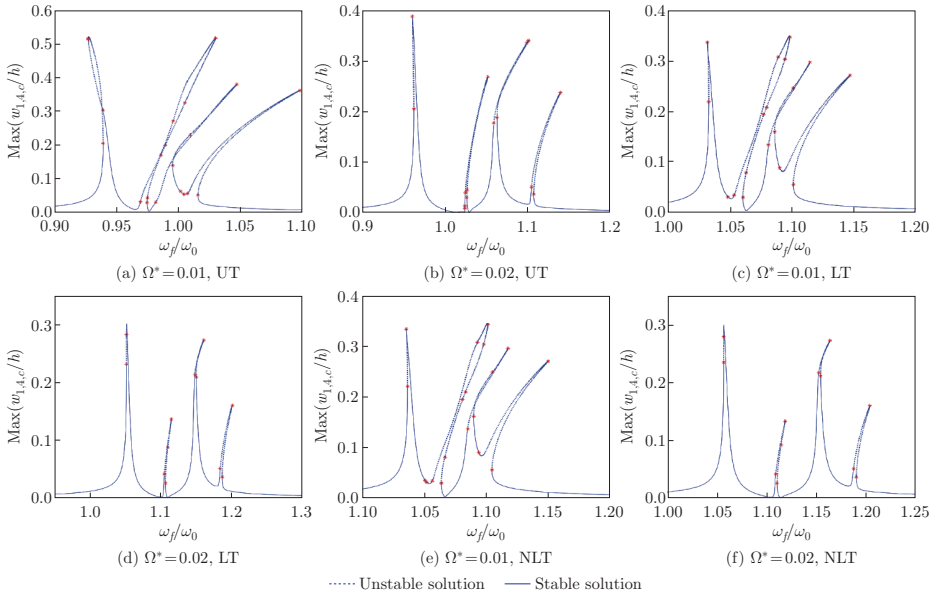

Fig. 9 Nonlinear amplitude-frequency response curves of the rotating composite shell for different dimensionless rotating speeds: (a), (c), and (e) $\Omega^* = 0.01$; (b), (d), and (f) $\Omega^* = 0.02$ (color online)

towards the direction of the larger dimensionless nonlinear frequency by increasing the porosity volume fraction. As the dimensionless nonlinear frequency increases, the amplitude peaks of the driving mode $w_{1,4,c}/h$ increase with the increase in the power-law index. Moreover, the nonlinear hardening/softening spring behaviors attenuate as the dimensionless rotating speed increases.

References

[1] BEHDINAN, K. and MORADI-DASTJERDI, R. Heat transfer behavior of graphene-reinforced nanocomposite sandwich cylinders. *Advanced Multifunctional Lightweight Aerostructures*: *Design*, *Development*, *and Implementation*, ASME-Wiley, eBooks, 25–42 (2021)

[2] MORADI-DASTJERDI, R. and BEHDINAN, K. Dynamic performance of piezoelectric energy harvesters with a multifunctional nanocomposite substrate. *Applied Energy*, **293**, 116947 (2021)

[3] LIU, Y., QIN, Z. Y., and CHU, F. L. Analytical study of the impact response of shear deformable sandwich cylindrical shell with a functionally graded porous core. *Mechanics of Advanced Materials and Structures*, **29**, 1338–1347 (2022)

[4] GUAN, X., ZHONG, R., QIN, B., WANG, Q., and SHUAI, C. A unified prediction solution for vibro-acoustic analysis of composite laminated elliptical shells immersed in air. *Journal of Central South University*, **28**, 429–444 (2021)

[5] LIU, Y. F., HU, W. Y., ZHU, R. Z., SAFAEI, B., QIN, Z. Y., and CHU, F. L. Dynamic responses of corrugated cylindrical shells subjected to nonlinear low-velocity impact. *Aerospace Science and Technology*, **121**, 107321 (2022)

[6] LIANG, F., LI, Z., YANG, X. D., ZHANG, W., and YANG, T. Z. Coupled bending-bending-axial-torsional vibrations of rotating blades. *Acta Mechanica Solida Sinica*, **32**, 326–338 (2019)

[7] YANG, J. H., YANG, X. D., QIAN, Y. J., and ZHANG, W. A novel type of bi-gyroscopic system undergoing both rotating and spinning motions. *Journal of Vibration and Acoustics*, **143**, 034502 (2021)

[8] LI, L., LUO, Z., HE, F. X., SUN, K., and YAN, X. L. An improved partial similitude method for dynamic characteristic of rotor systems based on Levenberg-Marquardt method. *Mechanical Systems and Signal Processing*, **165**, 108405 (2022)

[9] WANG, J., LIU, Y. F., QIN, Z. Y., MA, L., and CHU, F. L. Dynamic performance of a novel integral magnetorheological damper-rotor system. *Mechanical Systems and Signal Processing*, **172**, 109004 (2022)

[10] SAFAEI, B., SAHMANI, S., and ASL, H. T. Quasi-3D nonlinear flexural response of isogeometric functionally graded CNT-reinforced plates with various shapes with variable thicknesses. *Mechanics Based Design of Structures and Machines* (2021) https://doi.org/10.1080/15397734.2021.1999264

[11] ZENG, J., MA, H., YU, K., XU, Z. T., and WEN, B. C. Coupled flapwise-chordwise-axial-torsional dynamic responses of rotating pre-twisted and inclined cantilever beams subject to the base excitation. *Applied Mathematics and Mechanics* (*English Edition*), **40**(8), 1053–1082 (2019) https://doi.org/10.1007/s10483-019-2506-6

[12] KARROUBI, R. and IRANI-RAHAGHI, M. Rotating sandwich cylindrical shells with an FGM core and two FGPM layers: free vibration analysis. *Applied Mathematics and Mechanics* (*English Edition*), **40**(4), 563–578 (2019) https://doi.org/10.1007/s10483-019-2469-8

[13] SUN, S. P. and LIU, L. Multiple internal resonances in nonlinear vibrations of rotating thin-walled cylindrical shells. *Journal of Sound and Vibration*, **510**, 116313 (2021)

[14] LIU, Y. F., QIN, Z. Y., and CHU, F. L. Nonlinear dynamic responses of sandwich functionally graded porous cylindrical shells embedded in elastic media under 1:1 internal resonance. *Applied Mathematics and Mechanics* (*English Edition*), **42**(6), 805–818 (2021) https://doi.org/10.1007/s10483-021-2740-7

[15] DAI, Q. Y., LIU, Y. F., QIN, Z. Y., and CHU, F. L. Nonlinear damping and forced response of laminated composite cylindrical shells with inherent material damping. *International Journal of Applied Mechanics*, **13**, 2150060 (2021)

[16] LU, Z. Q., ZHANG, K. K., DING, H., and CHEN, L. Q. Nonlinear vibration effects on the fatigue life of fluid-conveying pipes composed of axially functionally graded materials. *Nonlinear Dynamics*, **100**, 1091–1104 (2020)

[17] YANG, S. W., HAO, Y. X., ZHANG, W., YANG, L., and LIU, L. T. Nonlinear vibration of functionally graded graphene platelet-reinforced composite truncated conical shell using first-order shear deformation theory. *Applied Mathematics and Mechanics* (*English Edition*), **42**(7), 981–998 (2021) https://doi.org/10.1007/s10483-021-2747-9

[18] DAI, Q. Y., LIU, Y. F., QIN, Z. Y., and CHU, F. L. Damping and frequency response characteristics of functionally graded fiber-reinforced composite cylindrical shells. *International Journal of Structural Stability and Dynamics*, **22**, 2250107 (2022)

[19] HAO, R. B., LU, Z. Q., DING, H., and CHEN, L. Q. A nonlinear vibration isolator supported on a flexible plate: analysis and experiment. *Nonlinear Dynamics*, **108**, 941–958 (2022)

[20] WANG, J., LIU, Y. F., QIN, Z. Y., MA, L., and CHU, F. L. Nonlinear characteristic investigation of magnetorheological damper-rotor system with local nonlinearity. *Chinese Journal of Aeronautics* (2022) https://doi.org/10.1016/j.cja.2022.06.001

[21] RAFIEE, M., NITZSCHE, F., and LABROSSE, M. Rotating nanocomposite thin-walled beams undergoing large deformation. *Composite Structures*, **150**, 191–199 (2016)

[22] GU, X. J., ZHANG, W., and ZHANG, Y. F. Nonlinear vibrations of rotating pretwisted composite blade reinforced by functionally graded graphene platelets under combined aerodynamic load and airflow in tip clearance. *Nonlinear Dynamics*, **105**, 1503–1532 (2021)

[23] LI, C. F., LI, P. Y., ZHONG, B. F., and MIAO, X. Y. Large-amplitude vibrations of thin-walled rotating laminated composite cylindrical shell with arbitrary boundary conditions. *Thin-Walled Structures*, **156**, 106966 (2020)

[24] KHOSRAVI, S., ARVIN, H., and KIANI, Y. Vibration analysis of rotating composite beams reinforced with carbon nanotubes in thermal environment. *International Journal of Mechanical Sciences*, **164**, 105187 (2019)

[25] LI, Z., ZHONG, R., WANG, Q. S., QIN, B., and YU, H. L. The thermal vibration characteristics of the functionally graded porous stepped cylindrical shell by using characteristic orthogonal polynomials. *International Journal of Mechanical Sciences*, **182**, 105779 (2020)

[26] LIU, T., ZHANG, W., MAO, J. J., and ZHENG, Y. Nonlinear breathing vibrations of eccentric rotating composite laminated circular cylindrical shell subjected to temperature, rotating speed and external excitations. *Mechanical Systems and Signal Processing*, **127**, 463–498 (2019)

[27] LIU, Y. F., QIN, Z. Y., and CHU, F. L. Nonlinear forced vibrations of FGM sandwich cylindrical shells with porosities on an elastic substrate. *Nonlinear Dynamics*, **104**, 1007–1021 (2021)

[28] LIU, Y. F., QIN, Z. Y., and CHU, F. L. Nonlinear forced vibrations of rotating cylindrical shells under multi-harmonic excitations in thermal environment. *Nonlinear Dynamics*, **108**, 2977–2991 (2022)

[29] AMABILI, M. *Nonlinear Mechanics of Shells and Plates in Composite, Soft and Biological Materials*, Cambridge University Press, New York (2018)

[30] LIU, Y. F., QIN, Z. Y., and CHU, F. L. Investigation of magneto-electro-thermo-mechanical loads on nonlinear forced vibrations of composite cylindrical shells. *Communications in Nonlinear Science and Numerical Simulation*, **107**, 106146 (2022)

[31] LIU, Y. F., QIN, Z. Y., and CHU, F. L. Nonlinear forced vibrations of functionally graded piezoelectric cylindrical shells under electric-thermo-mechanical loads. *International Journal of Mechanical Sciences*, **201**, 106474 (2021)

[32] DHOOGE, A., GOVAERTS, W., KUZNETSOV, Y. A., MEIJER, H. G. E., and SAUTOIS, B. New features of the software MatCont for bifurcation analysis of dynamical systems. *Mathematical and Computer Modelling of Dynamical Systems*, **14**, 147–175 (2008)

[33] CHEN, Y., ZHAO, H. B., SHEN, Z. P., GRIEGER, I., and KRÖPLIN, B. H. Vibrations of high speed rotating shells with calculations for cylindrical shells. *Journal of Sound and Vibration*, **160**, 137–160 (1993)

[34] AMABILI, M., PELLICANO, F., and PAIDOUSSIS, M. P. Nonlinear vibrations of simply supported, circular cylindrical shells, coupled to quiescent fluid. *Journal of Fluids and Structures*, **12**, 883–918 (1998)